machines

MDPI

Article

Numerical Simulation and Experiment on Excavating Resistance of an Electric Cable Shovel Based on EDEM-RecurDyn Bidirectional Coupling

Yinnan Feng [1,2,3], Juan Wu [1,2,3,*], Chenhao Guo [1,2,3] and Baoguo Lin [1,2,3]

1 College of Mechanical and Vehicle Engineering, Taiyuan University of Technology, Taiyuan 030024, China
2 Shanxi Province Engineer Technology Research Center for Mine Fluid Control, Taiyuan 030024, China
3 National-Local Joint Engineering Laboratory of Mining Fluid Control, Taiyuan 030024, China
* Correspondence: wujuan@tyut.edu.cn

Abstract: The electric cable shovel (ECS) is one of the core pieces of equipment used in open-pit mining, and the prediction of its excavating resistance is the basis and focus of optimization design, such as excavation trajectory planning and structure optimization of the ECS. Aiming to predict the excavating resistance of an ECS, a computer simulation method for the excavating resistance based on EDEM-RecurDyn bidirectional coupling simulation is proposed herein. Taking the China-made WK series ECS as the research object, a 1/30 scale model of the ECS was set up, a prototype model test bench of the ECS was built, and the kinematics solution and force analysis of the excavating process were carried out. According to the actual excavation conditions and excavating process of the ECS, a discrete element model of the material stack and a multibody dynamics model of the ECS prototype were established. The EDEM-RecurDyn bidirectional coupling simulation of the excavating process were realized using interface technology, and the excavating resistance levels under different speed combinations and different material repose angles were simulated and analyzed. In order to verify the accuracy of the simulation results, the feasibility and reliability of the EDEM-RecurDyn bidirectional coupling simulation were verified by physical experiments. The results show that the simulated excavating resistance is basically consistent with the excavating resistance measured in the experiment in terms of peak value and change trend, which verifies the feasibility and reliability of the EDEM-RecurDyn bidirectional coupling simulation to study the excavating resistance of an ECS.

Keywords: electric cable shovel (ECS); EDEM-RecurDyn co-simulation; excavating trajectory; excavating resistance; scale model

Citation: Feng, Y.; Wu, J.; Guo, C.; Lin, B. Numerical Simulation and Experiment on Excavating Resistance of an Electric Cable Shovel Based on EDEM-RecurDyn Bidirectional Coupling. *Machines* **2022**, *10*, 1203. https://doi.org/10.3390/machines10121203

Academic Editor: Antonio J. Marques Cardoso

Received: 5 November 2022
Accepted: 6 December 2022
Published: 12 December 2022

1. Introduction

An electric cable shovel (ECS), also known as a rope shovel, is a mechanical excavator that is widely used in ore mining operations of open-pit minerals, and is one of the key pieces of equipment for open-pit mining [1]. In recent years, with the increasing demand for ore resources at home and abroad, the production scale of open-pit ores has gradually expanded, and higher requirements have been put forward for electric shovels [2]. Excavating resistance analysis has always been the basis for all kinds of excavation equipment to carry out excavating trajectory planning, structural optimization, vibration, power consumption, and other calculations. Therefore, accurately predicting the excavating resistance of the electric shovel is particularly critical.

At present, the discrete element method is one of the main methods for scholars at home and abroad to study excavating resistance; it is mainly based on discrete element software. According to the parameters of the material that is to be excavated, the material particle model is set up in the simulation software, and an analysis method is used to simulate the actual excavating process through computer simulation. Coetzee, C.J. [3,4] verified the accuracy of the discrete element method in predicting the full rate of excavator buckets through experiments, and the experimental results showed that the error of the full dipper rate predicted by the discrete element method was within 6% at all stages of loading. Huang et al. [5] realized the visualization of a loader loading process based on EDEM software, and they compared the movement rules of different particle-size materials by simulating the excavating process of such materials. Meng et al. [6] compared the four different shoveling methods of the LHD through EDEM simulation and proposed an optimization scheme for the bucket trajectory to improve the efficiency of the scraping operation. Zhao Lijuan et al. [7,8] simulated the cutting process of a shearer based on DEM–MBD simulation, and they built a test platform based on a similar theory to verify the feasibility of the simulation and the reliability of the results. Bi Qiushi et al. [9,10] proposed a numerical simulation method for electric shovel excavating resistance and excavating energy consumption based on EDEM-ADAMS co-simulation; they simulated and calculated the excavation resistance and excavating energy consumption, and built an experimental prototype to verify the accuracy of the numerical simulation results; however, when analyzing excavation performance, they set the crowd speed and hoist speed to a uniform speed to simplify the calculation, without considering the acceleration and deceleration process, and without analyzing the influence of different material repose angles on excavation performance.

Aiming at the problem of predicting electric shovel excavating resistance, in this paper, we take the China-made WK series ECS as the research object, we set up a 1/30 ECS scale model based on a similar theory, and perform kinematic solution and force analysis of the excavating process. It is difficult to accurately predict the interaction between the dipper and material particles with a single EDEM discrete element simulation or RecurDyn multibody dynamics simulation. Therefore, in this paper, we establish a discrete element model of the excavated material in EDEM and a multibody dynamic model of the prototype model in RecurDyn, we simulate the excavating process of the ECS by EDEM-RecurDyn bidirectional coupling simulation, and the excavating resistance under different speed combinations and different material repose angles is simulated and analyzed.

In order to verify the feasibility and reliability of the research method, the ECS scale model test bench was built and used to carry out the excavation test. By comparing the simulation results with the test results, it was found that the simulated excavating resistance is basically consistent with the measured excavating resistance in peak value and change trend under various working conditions, which verifies that EDEM-RecurDyn bidirectional coupling simulation can accurately predict the excavating resistance of the ECS.

2. EDEM-RecurDyn Co-Simulation Method

2.1. Construction of the Electric Shovel Scale Model

In order to facilitate the simulation and analysis of the ECS excavating process, a 3D model of the WK series ECS produced by the Taiyuan Heavy Machinery Group was established, as shown in Figure 1a. However, the size of the model was too large, the time required for co-simulation was too long, and it was difficult to verify the simulation results experimentally. Therefore, in order to improve the simulation efficiency and facilitate experimental verification on the basis of this model, a scale model of the ECS was established based on similarity theory with a scale of 1/30. This is shown in Figure 1b.

This paper refers to the size of the China-made WK series ECS, based on the similarity theory, the real shovel is scaled at a ratio of 1/30 to determine the specific structural parameter values [10–12]. The meanings of the structural parameters corresponding to the front-end working device of the ECS scale model are shown in Figure 2, and the specific values of each parameter and the geometric dimensions of the dipper are presented in Table 1.

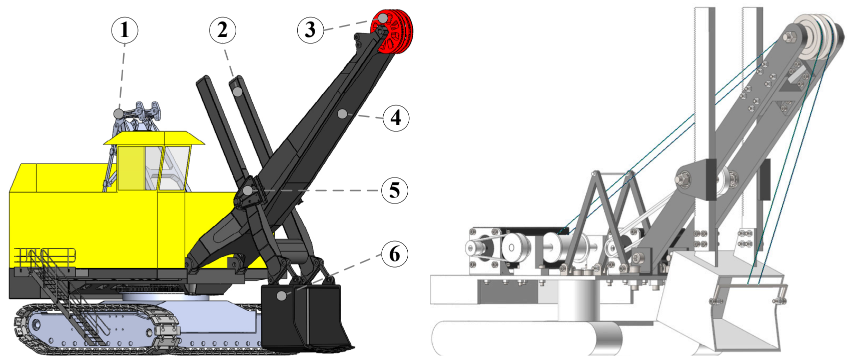

(**a**) (**b**)

Figure 1. ECS model and ECS scale model: (**a**) an ECS model and its main structural members (① A frame, ② dipper handle, ③ boom point sheave, ④ boom, ⑤ saddle block, ⑥ dipper); (**b**) a 1/30 scale model of the ECS.

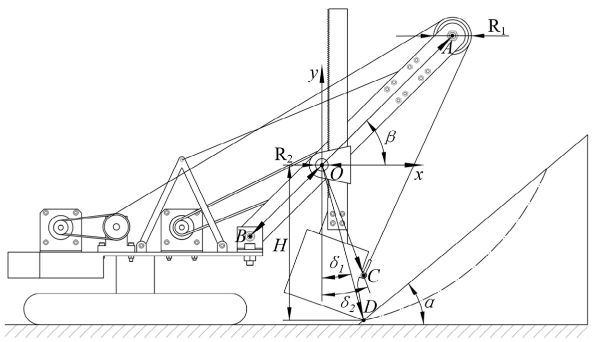

Figure 2. Structural parameters of the ECS scale model: R_1—boom point sheave diameter; R_2—crowd gear diameter; l_{AB}—boom length; l_{OB}, l_{OC}, l_{OD}—the distances from the rotation center of the saddle to the bottom of the boom, the hoist beam, and the tooth tip; H—height of saddle rotation center from tooth tip; α—material angle of repose; β—angle between boom and horizontal direction; δ_1, δ_2—angle between l_{OD}, l_{OC} and the parallel direction of the dipper handle.

Table 1. Structural parameter values.

Parameter (Unit)	Value	Parameter (Unit)	Value
R_1 (mm)	58	H (mm)	247.3
R_2 (mm)	20	α (°)	40
l_{AB} (mm)	450	β (°)	45
l_{OB} (mm)	160	δ_1 (°)	14.8
l_{OC} (mm)	186.5	δ_2 (°)	20.43
l_{OD} (mm)	255.8	Dipper (mm)	120 × 110 × 100

2.2. Kinematic Solution of the Electric Shovel Scale Model

The working process of the ECS can be divided into four steps: excavation, rotation, unloading, and returning. This paper mainly analyzes the excavating process. In the process of excavation, the rotary and walking mechanism of the ECS does not work, and the boom is fixed, that is, the pose of the boom in the coordinate system {B} is determined. So, the ECS scale model can be regarded as a 1R-1P system, that is, the rotational motion of the dipper handle around the ξ_1 direction and the prismatic motion along the ξ_2 direction, as shown in Figure 3a.

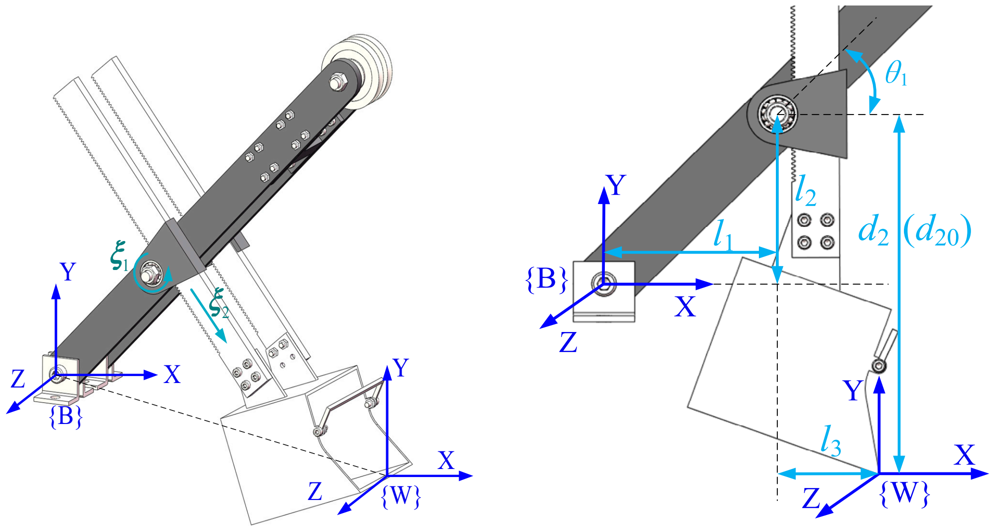

(**a**) (**b**)

Figure 3. Establishment of the coordinate system of the scale model: (**a**) general posture; (**b**) initial posture (l_1, l_2–horizontal and vertical distance from the saddle rotation center to the origin of coordinate system {B}; l_3–the distance from the saddle rotation center to dipper tooth tip in vertical direction of the dipper handle; θ_1–the dipper handle rotation angle; d_2–the dipper handle elongation; d_{20}–initial value of the dipper handle elongation).

In this paper, kinematic modeling analysis of the electric shovel is accomplished based on the product of exponentials [13]. The structure of the platform is presented in Figure 3a, and we establish the base coordinate system {B} and target coordinate system {W} as shown. Prior to the kinematics model, the following process variables are introduced: $T_{BW}(q)$ represents the homogeneous transformation matrix of the target coordinate system {W} relative to the base coordinate system {B}; $T_{BW}(0)$ represents the initial pose homogeneous transformation matrix of the target coordinate system relative to the machine coordinate system; ξ_1 and ξ_2 denote the representations of the actual spinor of the A-axis and C-axis in the base coordinate system {B}, respectively. Thus, the forward kinematics model from the platform-based coordinate system to the target coordinate system is

$$T_{BW}(q) = e^{[\hat{\xi}_1]\theta_1} e^{[\hat{\xi}_2]d_2} T_{BW}(0) \tag{1}$$

For the axis of rotation, the spinor is $\xi = (\omega, v)^T$, $v = r \times \omega$, and the spinor of the translation axis is $\xi = (0, v)^T$, where ω denotes the orientation vector of the rotation axis, which is a unit vector. Where r represents any point on the rotation axis. The specific motion matrix form of the rotation axis is mathematically expressed as

$$\begin{cases} e^{[\hat{\xi}]\theta} = \begin{bmatrix} e^{[\hat{\omega}]\theta} & \left(I - e^{[\hat{\omega}]\theta}\right)(\hat{\omega} \times v) + \hat{\omega}\hat{\omega}^T v\theta \\ 0_{1\times 3} & 1 \end{bmatrix}, \hat{\omega} \neq 0 \\ e^{[\hat{\xi}]\theta} = \begin{bmatrix} I & \hat{v}\theta \\ 0 & 1 \end{bmatrix}, \hat{\omega} = 0 \end{cases} \tag{2}$$

Obviously,

$$\begin{cases} \hat{\omega}_1 = \begin{pmatrix} 0 & 0 & 1 \end{pmatrix}^T \\ \hat{v}_2 = \begin{pmatrix} 0 & -1 & 0 \end{pmatrix}^T \end{cases} \tag{3}$$

$$T_{BW}(0) = \begin{bmatrix} 1 & 0 & 0 & l_1 + l_3 \\ 0 & 1 & 0 & -d_{20} + l_2 \\ 0 & 0 & 1 & 0 \\ 0 & 0 & 0 & 1 \end{bmatrix} \tag{4}$$

Combined with the relative position relationship of the coordinate system in Figure 3b, it can be calculated that

$$\begin{cases} \hat{\xi}_1 = \begin{pmatrix} 0 & 0 & 1 & l_2 & -l_1 & 0 \end{pmatrix}^T \\ \hat{\xi}_2 = \begin{pmatrix} 0 & 0 & 0 & 0 & -1 & 0 \end{pmatrix}^T \end{cases} \tag{5}$$

Therefore,

$$T_{BW}(q) = e^{[\hat{\xi}_1]\theta_1} e^{[\hat{\xi}_2]d_2} T_{BW}(0) = \begin{bmatrix} \cos\theta_1 & -\sin\theta_1 & 0 & l_3\cos\theta_1 + l_1 + d_2\sin\theta_1 + d_{20}\sin\theta_1 \\ \sin\theta_1 & \cos\theta_1 & 0 & l_3\sin\theta_1 + l_2 - d_2\cos\theta_1 - d_{20}\cos\theta_1 \\ 0 & 0 & 1 & 0 \\ 0 & 0 & 0 & 1 \end{bmatrix} \tag{6}$$

The values of l_1, l_2, and l_3 are determined by the body structure of the ECS scale model itself. Therefore, the position and attitude of the dipper tooth tip relative to the body can be obtained through the values of the θ_1 and d_2, thus, completing the solution of the kinematic positive problem.

The solution of the kinematic inverse problem of the ECS scale model is to solve the values of the joint variables θ_1 and d_2 according to the posture of the dipper tooth tip. Therefore, the body posture transformation matrix $\boldsymbol{T}$ can be set to

$$T = \begin{bmatrix} r_{11} & r_{12} & r_{13} & t_x \\ r_{21} & r_{22} & r_{23} & t_y \\ r_{31} & r_{32} & r_{33} & t_z \\ 0 & 0 & 0 & 1 \end{bmatrix} \tag{7}$$

$$r = \begin{bmatrix} r_{11} & r_{12} & r_{13} \\ r_{21} & r_{22} & r_{23} \\ r_{31} & r_{32} & r_{33} \end{bmatrix}, t = \begin{bmatrix} t_x \\ t_y \\ t_z \end{bmatrix} \tag{8}$$

where $\boldsymbol{r}$ is the rotation change matrix from the body to the dipper tooth; $\boldsymbol{t}$ is the translation change matrix and can be obtained by comparing Formulas (6) and (7).

$$\begin{aligned} t_x &= l_3 \cos\theta_1 + l_1 + d_2 \sin\theta_1 + d_{20} \sin\theta_1 \\ t_y &= l_3 \sin\theta_1 + l_2 - d_2 \cos\theta_1 - d_{20} \cos\theta_1 \end{aligned} \tag{9}$$

The expression of the dipper handle rotation angle θ_1 and the dipper handle elongation d_2 can be obtained from the above equation.

$$\theta_1 = \arctan\left(\frac{(t_y - l_2)l_3 + (t_x - l_1)(d_2 + d_{20})}{(t_x - l_1)l_3 - (t_y - l_2)(d_2 + d_{20})} \right) (\theta_1 \neq 90^0) \tag{10}$$

$$d_2 = \sqrt{(t_x - l_1)^2 + (t_y - l_2)^2 - l_3{}^2} - d_{20} \tag{11}$$

When the body posture transformation matrix T is known, the values of θ_1 and d_2 can be obtained by Equations (10) and (11), thus, solving the kinematic inverse problem.

2.3. Force Analysis of the Excavating Process of the ECS Scale Model

The force on the front working device of the ECS during excavation is shown in Figure 4: point A is the center of gravity of the dipper handle; point F is the center of gravity of the dipper; F_1 is the supporting force of the crowd gear on the dipper handle; F_{tui} is the crowd force of the dipper handle; F_{ti} is the rope hoist force; F_τ and F_n are, respectively, the tangential and the normal excavating resistances of the dipper tooth tip; G_1 is the gravity of the dipper handle; G_2 is the gravity of the dipper and the material. We simplify the gravity center of the excavated material to the gravity center of the dipper for calculation purposes.

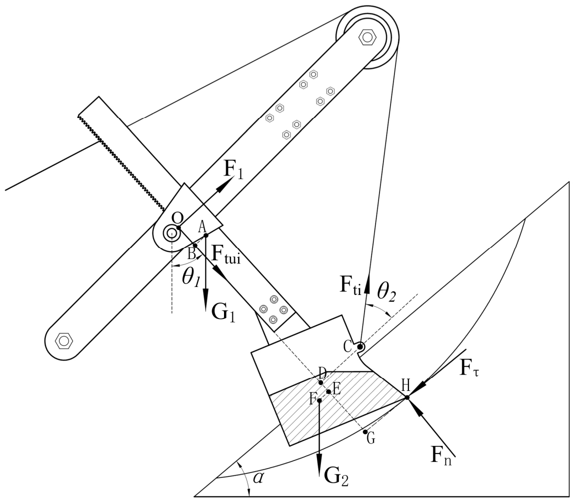

Figure 4. Force analysis of the excavation process.

The tangential excavating resistance F_τ can be further decomposed into three parts, including the lower lip excavating resistance F_{11}, the resistance caused by speed F_{12}, and the resistance generated by the material extrusion on both sides of the wall F_{13} [12].

$$F_\tau = F_{11} + F_{12} + F_{13} \tag{12}$$

For F_{11}, what can be obtained is as follows [14]:

$$\begin{cases} F_{11} = \sigma(\gamma g d^2 N_\gamma + c d N_c + \gamma v^2 d N_a) \\ N_\gamma = 0.5(\cot\varepsilon + \cot\alpha)/E_N \\ N_c = [1 + \cot\alpha\cot(\alpha+\varphi)]/E_N \\ N_a = [\tan\alpha + \cot(\alpha+\varphi)]/[1 + \tan\alpha\cot\varepsilon/E_N] \\ E_N = \cos(\varepsilon+\psi) + \sin(\varepsilon+\psi)\cot(\alpha+\varphi) \\ \alpha = (\pi - \varphi) \end{cases} \tag{13}$$

where σ is the dipper width, γ is the material density, d is the excavating depth, c is the material cohesion, v is the speed of the dipper teeth, ε is the digging angle, α is the material angle of repose, φ is the internal friction angle of the material, ψ is the mechanical-soil friction angle.

Following references [1,14], F_{12} and F_{13} can be calculated through (14) and (15):

$$F_{12} = \frac{\sigma d v^2 \gamma[\tan\alpha\sin(\alpha+\varphi) + \cos(\alpha+\varphi)]}{\sin(\varepsilon+\psi+\alpha+\varphi)(1+\tan\alpha\cot\varepsilon)} \tag{14}$$

$$F_{13} = \frac{2d^3\gamma(\cot\varepsilon + \cot\alpha)\sin(\varepsilon+\psi)\sqrt{\cot^2\alpha + \cot\varepsilon\cot\alpha}}{3\sigma\sin(\varepsilon+\alpha+\varphi+\psi)} \tag{15}$$

The normal excavating resistance F_n perpendicular to the speed of the dipper teeth is produced by the extrusion reaction between the dipper and the material, so it can be derived in terms of the corresponding material properties of the dipper and material [1].

$$F_n = \frac{F_\tau \tan\psi}{1 - \zeta\tan\psi} \tag{16}$$

where ζ is the proportionality coefficient and usually among 0.3∼0.45 [1].

According to the static equilibrium principle, the combined torque of all external forces on the dipper handle and the dipper assembly to the instantaneous meshing point O is zero; therefore,

$$\sum M_0(F_i) = 0 \tag{17}$$

Substituting each variable into Equation (17), we obtain:

$$F_{ti} = \frac{F_\tau r_\tau + G_1 r_1 + G_2 r_2 - F_n r_n}{r_{ti}} \tag{18}$$

where $r_\tau = l_{OG}$;
$r_n = l_{GH}$;
$r_1 = l_{OB} \sin\theta_1 + l_{AB} \cos\theta_1$;
$r_2 = l_{OE} \sin\theta_1 - l_{EF} \cos\theta_1$;
$r_{ti} = l_{OD} \cos\theta_2 + l_{CD} \sin\theta_2$.

The projection of the external force on the dipper handle and dipper in the direction of the straight line OG is zero; therefore,

$$\sum F_i = 0 \tag{19}$$

By substitution of each variable into Equation (19), we obtain:

$$F_{tui} = F_{ti} \sin\theta_2 + F_n - G_1 \cos\theta_1 - G_2 \cos\theta_1 \tag{20}$$

2.4. Establishment of a Discrete Element Model of Materials Based on EDEM

The main material excavated by the ECS under actual working conditions is the ore after blasting; the vast majority of particle sizes are between 200 and 400 mm, and the maximum particle size of individual ores is 900 mm. Since the size of the ECS scale model is 1/30 of the actual size of the ECS, the excavated material used during the test process should have the same scale [15]. Therefore, in the process of test verification, 10–30 mm limestone particles were selected as the material to be excavated. To improve the accuracy of the EDEM simulation, a 3D model of the limestone particles was established with reference to the shape of the limestone particles, as shown in Figure 5b. Then it was imported into the EDEM software and in order to improve the efficiency of the simulation, it is filled with four spherical particles, as shown in Figure 5c. The set particle size was 10 to 30 mm, and the mass fraction of each particle size is shown in Figure 6.

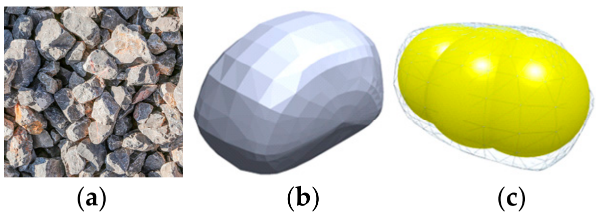

Figure 5. Establishment of particle models: (**a**) The limestone particles; (**b**) 3D model of the limestone particles; (**c**) The material particle in EDEM.

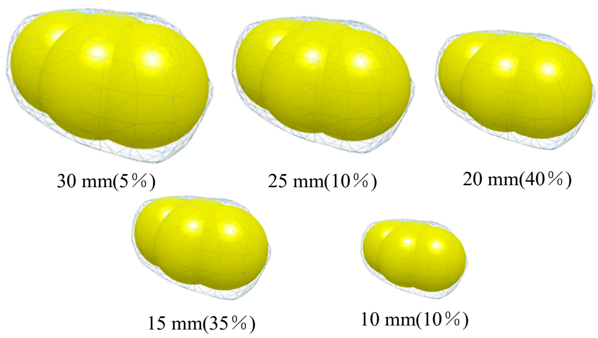

Figure 6. Particle size distribution.

The main performance parameters of the material are particle size, Poisson's ratio, density, shear strength, cohesion, internal friction angle, compressive strength, etc. Among them, shear strength, density, Poisson's ratio and related contact parameters play a major role in EDEM simulation analysis [16–21]. Therefore, following reference [9], we set the material properties of the particles and contact parameters of the dipper as shown in Tables 2 and 3.

Table 2. Material properties of the pellets and bucket.

Material	Poisson's Ratio	Shear Modulus (MPa)	Density (kg/m^3)
Particles	0.35	1.35×10^3	2540
Bucket	0.30	7.9×10^4	7800

Table 3. Contact parameters of materials.

Material	Coefficient of Restitution	Coefficient of Static Friction	Coefficient of Rolling Friction
Particle-Particle	0.65	0.30	0.08
Particle-Bucket	0.65	0.28	0.07

Since the natural accumulation angle of the ore after blasting is about 40° [22–26], in order to verify whether the material parameters are reasonable, the natural accumulation surface of the material was simulated by EDEM. Firstly, we added a square box with a length, width, and height of 500 mm in EDEM to stack the particles, and we filled it with the set material particles. Secondly, after the particles had stabilized, we removed one side of the box and let the material slide freely under the force of gravity to form a repose angle. Finally, after the particles in the box stopped slipping and the speed became zero, the natural accumulation angle of the material was measured. The process is shown in Figure 7.

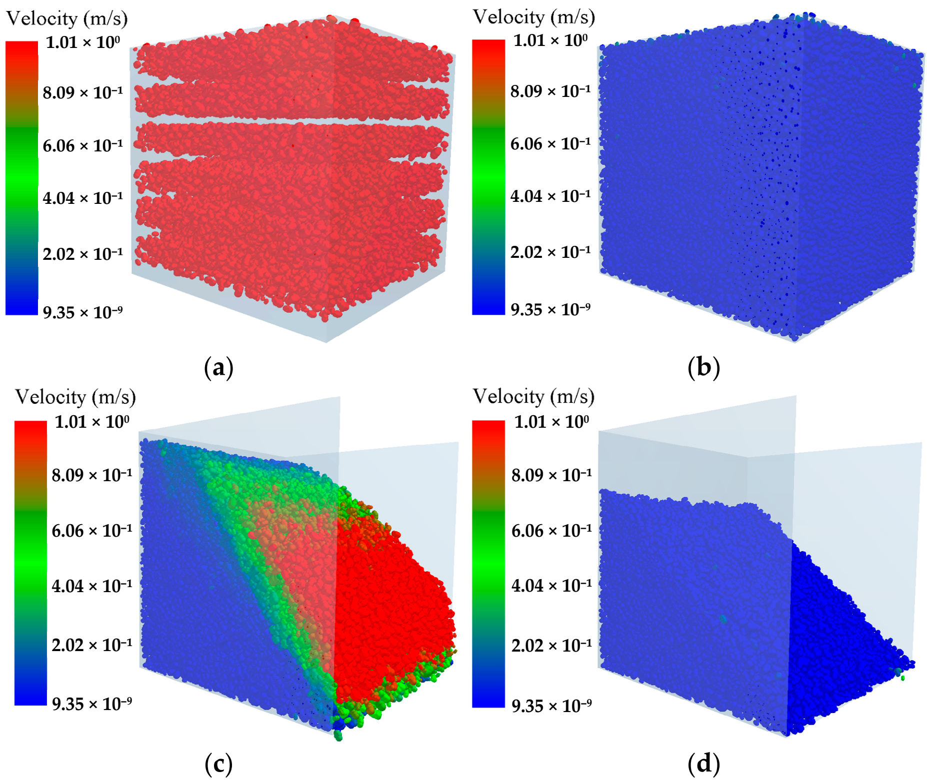

Figure 7. The simulation process of the natural accumulation surface of the materials: (**a**) Material filling process; (**b**) Material stabilization process; (**c**) Free slipping process; (**d**) Material stops slipping.

In the above figure, the particle color is used to represent the movement speed of the particle, and the color changes from blue to red as the particle velocity gradually increases. The natural accumulation angle of the material was measured by the angle measurement function in the EDEM post-processing module, and the measured repose angle was 39.88°, as shown in Figure 8. Therefore, the parameters of the particles were set reasonably, and the next step of the excavating process simulation could be carried out.

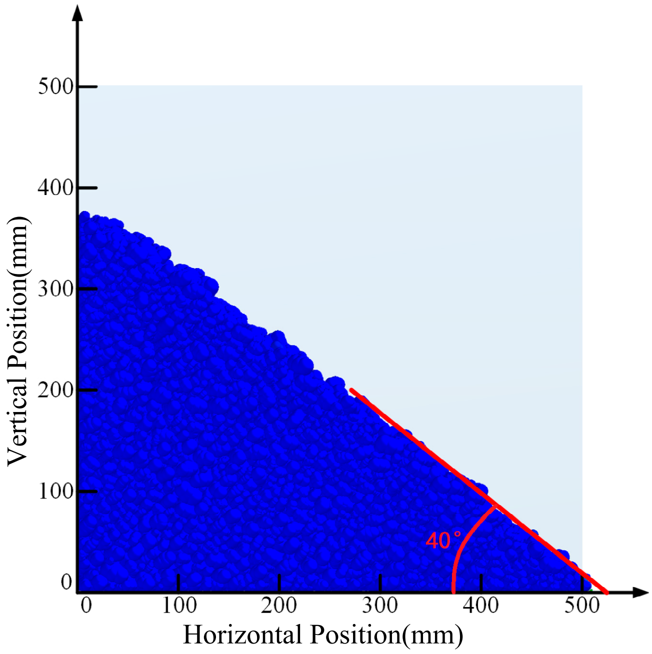

Figure 8. Measurement of the natural accumulation angle.

2.5. Establishment of a Multibody Dynamics Model Based on RecurDyn

We used SolidWorks to establish individual components of the ECS scale model and perform assembly and interference checking. The completed shovel scale model was imported into RecurDyn, and RecurDyn was used to add material properties, constraints, loads, and other simulation parameters to each part. Secondly, according to the classification of the kinematic pairs in RecurDyn and the actual motion of the ECS excavating process, the kinematic pair constraints between the components were defined as shown in Figure 9 and Table 4; the spherical pair constraint was added between the hoist rope, the hoist beam and the rollers; the FCur-Sur contact was added between the hoist rope and the boom point sheave and the rollers to simulate the characteristics of the hoist rope. Since the excavating process of the ECS is mainly achieved by the crowd motion of the dipper handle and the hoist motion of the hoist rope, the prismatic pair between the dipper handle and the saddle and the revolute pair between the hoist drum and the dipper were added to the drive. The change trend for the crowd speed and hoist speed can be divided into three stages: acceleration, uniform speed, and deceleration. In order to reduce the sudden change in driving force caused by acceleration mutation, a smooth transition should be ensured at the corner of the speed, so the step driving function was used to set the crowd and hoist speed. The set driving functions are shown in Table 5.

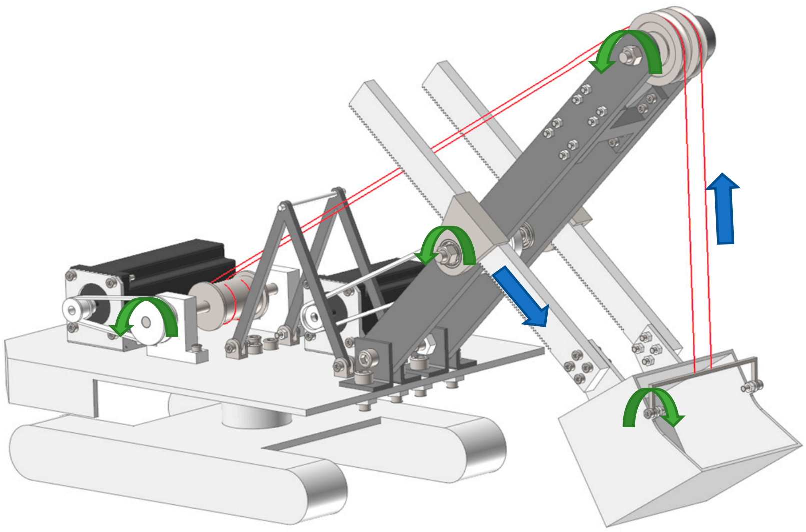

Figure 9. Movement pair settings.

Table 4. Kinematic pair constraints.

Component	Kinematic Pair	Component	Kinematic Pair
Saddle block–Boom	Revolute pair	Boom point sheave–Boom	Revolute pair
Dipper handle–Saddle	Prismatic pair	Hoist beam–Dipper	Revolute pair
Hoist drum–Bracket	Revolute pair		

Table 5. Driving function settings.

Speed Combination	Excavating Time	Crowd Driving Function	Hoist Driving Function
High-speed excavation	9 s	step (time, 0, 0, 3, 30) + step (time, 6, 0, 9, −30)	step (time, 0, 0, 3, 15D) + step (time, 6, 0, 9, −15D)
Medium-speed excavation	12 s	step (time, 0, 0, 3, 20) + step (time, 9, 0, 12, −20)	step (time, 0, 0, 3, 10D) + step (time, 9, 0, 12, −10D)
Low-speed excavation	18 s	step (time, 0, 0, 3, 12) + step (time, 15, 0, 18, −12)	step (time, 0, 0, 3, 6D) + step (time, 15, 0, 18, −6D)

2.6. EDEM and RecurDyn Bidirectional Coupling Simulation Analysis Process

The excavating process of the ECS is the result of multifactor coupling. The geometric parameters of the working mechanism, the kinematic parameters, the rock characteristics of the material, and the interaction between the dipper and the material directly or indirectly affect the excavation process and the kinetic characteristics of the ECS, so the DEM–MBD bidirectional coupling principle was used to build a bidirectional coupling model of the ECS scale model excavating the discrete element material based on the interface between EDEM and RecurDyn.

The bidirectional coupling simulation of EDEM-RecurDyn is within any time step of EDEM. RecurDyn transmits the kinematic parameters, such as displacement, velocity, and acceleration of the coupling components calculated in the time step to the corresponding coupling parts in EDEM, which then recalculates the influence of the coupling components' position change on the force, position, speed, and other parameters of the material particles. According to discrete element theory, the force and torque of the material particles on the coupling components are calculated, and the data are transmitted back to RecurDyn; RecurDyn finally recalculates the dynamic parameters of the coupling components according to the theory of multibody dynamics, thus, completing the bidirectional coupling transmission of data in a single-time step and so on until the end of the simulation.

In the excavating process, only the dipper and the excavated material will have an interaction force, and the rest of the components and the material will not interact, so in order to improve the simulation efficiency, the walls and export functions under the External

SPI module in RecurDyn were used to export the dipper as a wall file; the generated wall file was imported into the EDEM environment; and the simulation parameters were set. We entered the simulation interface to open the coupling interface to perform the bidirectional coupled simulation of EDEM-RecurDyn. The bidirectional coupled simulation process of the ECS scale model dipper is shown in Figure 10.

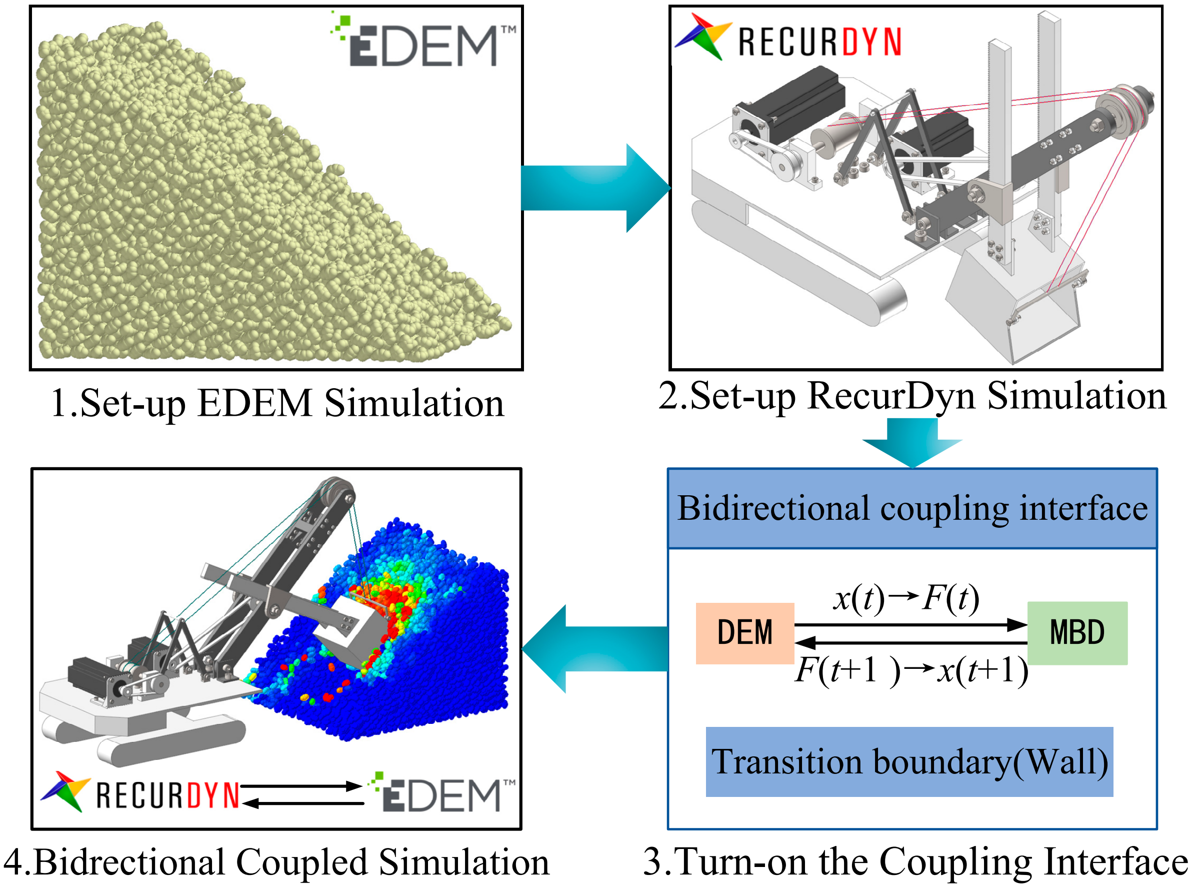

Figure 10. Bidirectional coupled simulation process.

3. Simulation Result Analysis

3.1. Simulation Result Analysis under Different Speed Combinations

By the method of EDEM-RecurDyn bidirectional coupling, the excavating process under different speed combinations was simulated and analyzed, and the simulation results are shown in Figure 11. From Figure 11a, it can be seen that the excavating resistance changes trend under different speed combinations, the size of the peak, and the location of its occurrence are basically the same, which is because the excavating resistance is mainly affected by the excavating depth, and the impact of the speed is very small. The selected speed combination basically has a consistent excavating trajectory, and the maximum excavating depth and its location are basically the same. From Figure 11c,d, it can be seen that with increasing speed, the crowd power and hoist power also increase, and the hoist power is about two times the crowd power, explaining that the hoist motion plays a leading role in the excavating process.

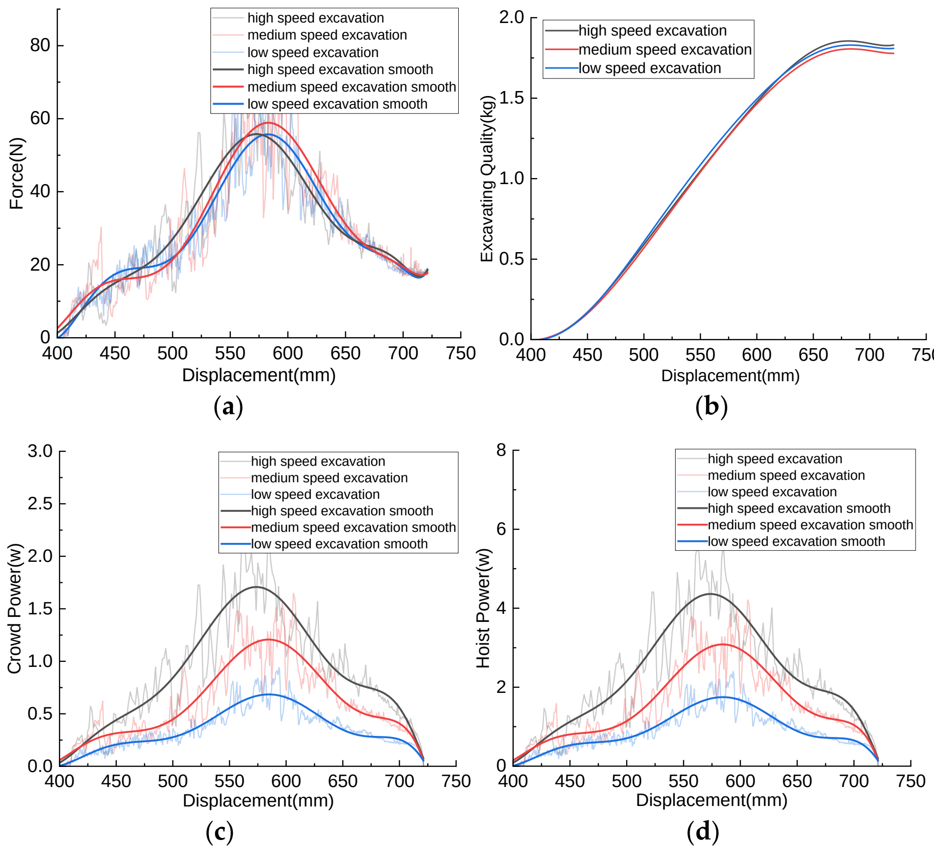

Figure 11. Comparison of simulation results under different speed combinations: (**a**) Excavating resistance; (**b**) Excavating quality; (**c**) Crowd power; (**d**) Hoist power.

3.2. Analysis of Simulation Results at Different Repose Angles

Due to the repose angle of the material after blasting being complex and changeable, not necessarily the 40° repose angle, in order to analyze the excavating performance of the ECS in different working environments, the ECS excavating process at different material repose angles (35, 40, and 45°) was simulated. First of all, for changing the restitution coefficient, static friction coefficient, and rolling friction coefficient between the material particles to generate different repose angles, the corresponding angle parameter settings are shown in Table 6.

Table 6. Settings of material contact parameters.

Stacking Angle	Coefficient of Restitution	Coefficient of Static Friction	Coefficient of Rolling Friction
35°	0.6	0.25	0.07
40°	0.65	0.3	0.08
45°	0.4	0.43	0.09

Under the condition of ensuring that the quality of a single excavation is basically the same, the crowd and hoist speeds of different material surfaces were determined by a trial-and-error method, as shown in Figure 12a,b, and the corresponding excavating trajectories under different material surfaces are shown in Figure 12c. It can be intuitively seen from the figure that with increasing repose angle, the hoist speed of the hoist rope gradually increases, while the crowd speed of the dipper handle decreases. This is due to the fact that, with an increasing repose angle, the distance between the material and the ECS itself is shortened, and the distance that the dipper needs to extend when digging the material is also shortened; in order to ensure that the dipper can smoothly detach from the material stacking surface, hoist ropes need to be retracted for longer lengths.

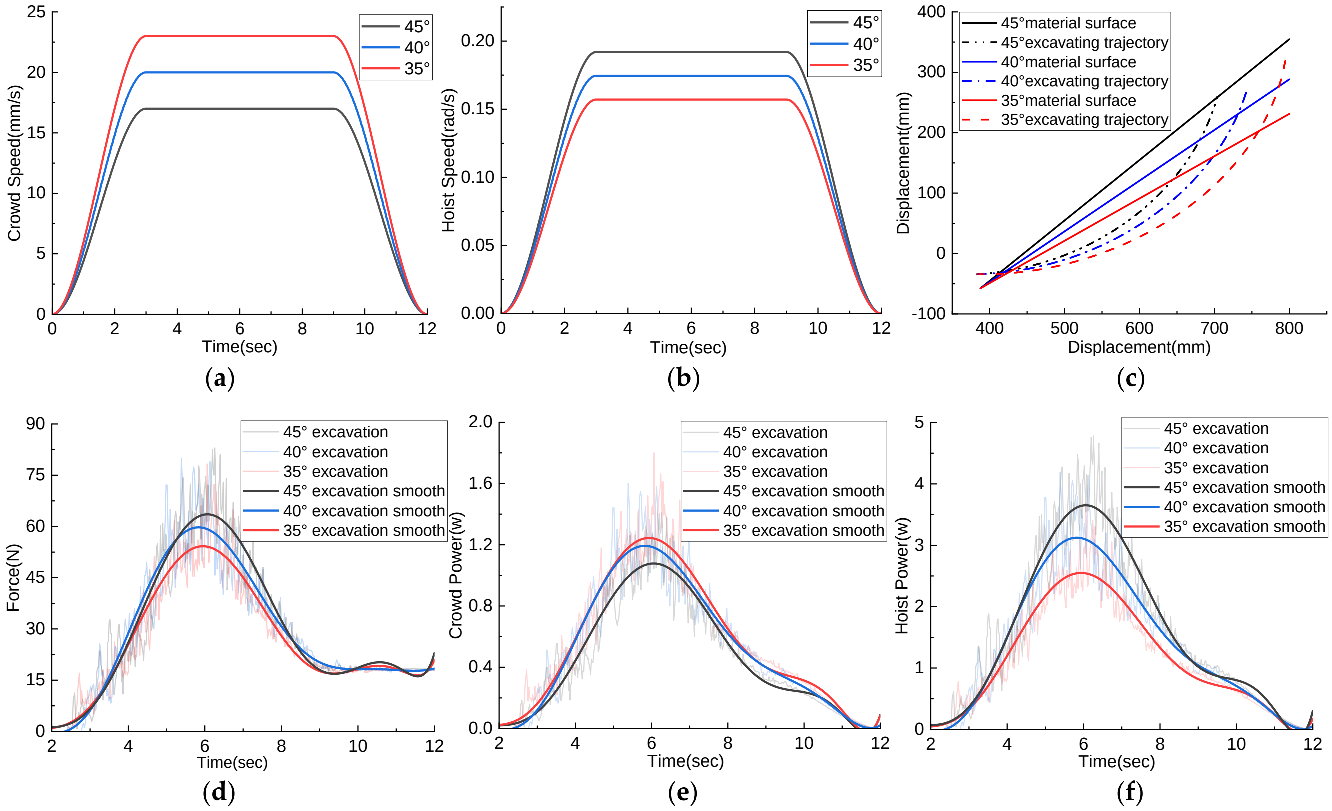

Figure 12. Comparison of simulation results under different stacking angles: (**a**) Crowd speed; (**b**) Hoist speed; (**c**) Excavating trajectory; (**d**) Excavating resistance; (**e**) Crowd power; (**f**) Hoist power.

Figure 12d–f presents the trends in excavating resistance, crowd power, and hoist power with time when the ECS scale model excavates at different repose angles. It can be seen from the figure that with increasing material repose angle, the maximum excavating resistance and the maximum hoist power increase, while the maximum crowd power decreases; the change trend of each parameter with time under different repose angles is basically the same.

4. Analysis of Test Results

The degree of coincidence between the simulation results obtained based on the EDEM–RecurDyn bidirectional coupling simulation and the experimental results obtained by physical experiments determines the theoretical and practical significance of using this method to study the ECS excavating process. Therefore, in this paper, an ECS scale model test bench (see Figure 13) was set up to conduct excavating experiments, and the feasibility and reliability of the research method were verified by comparing the simulation results with the test results.

The drive system and sensor measurement system of the test bench are shown in Figure 14. The crowd and hoist motion of the test prototype excavation device was realized by two separate motor drive systems, and control of the motor was achieved using the upper machine LabVIEW software and single-chip microcomputer control of the motor encoder. A dynamic torque sensor was used to measure the dipper handle crowd force in real time, a tensile force sensor was used to measure the rope hoist force in real time, and a rotary encoder was used to measure the dipper handle elongation and the hoist rope lift capacity. LabVIEW software works with a data logger to capture, store, and display sensor measurement data. The test bench system structure is shown in Figure 15.

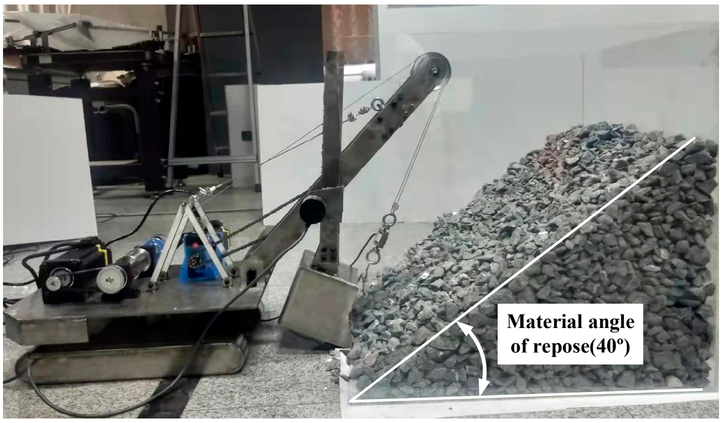

Figure 13. Electric shovel scale model test bench.

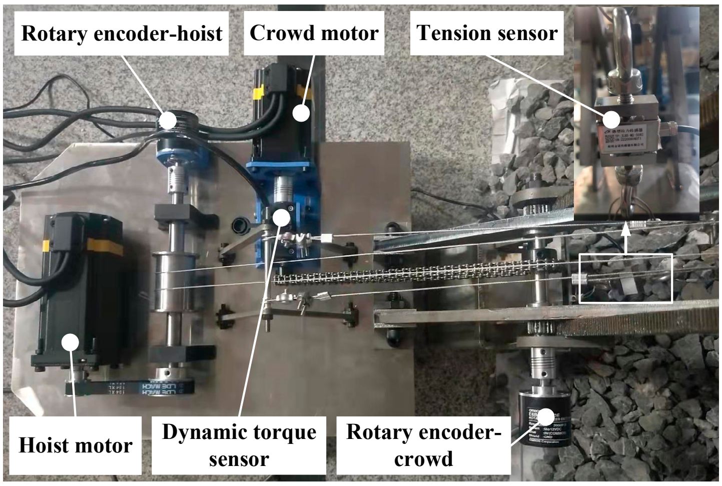

Figure 14. Motor and sensor installation positions.

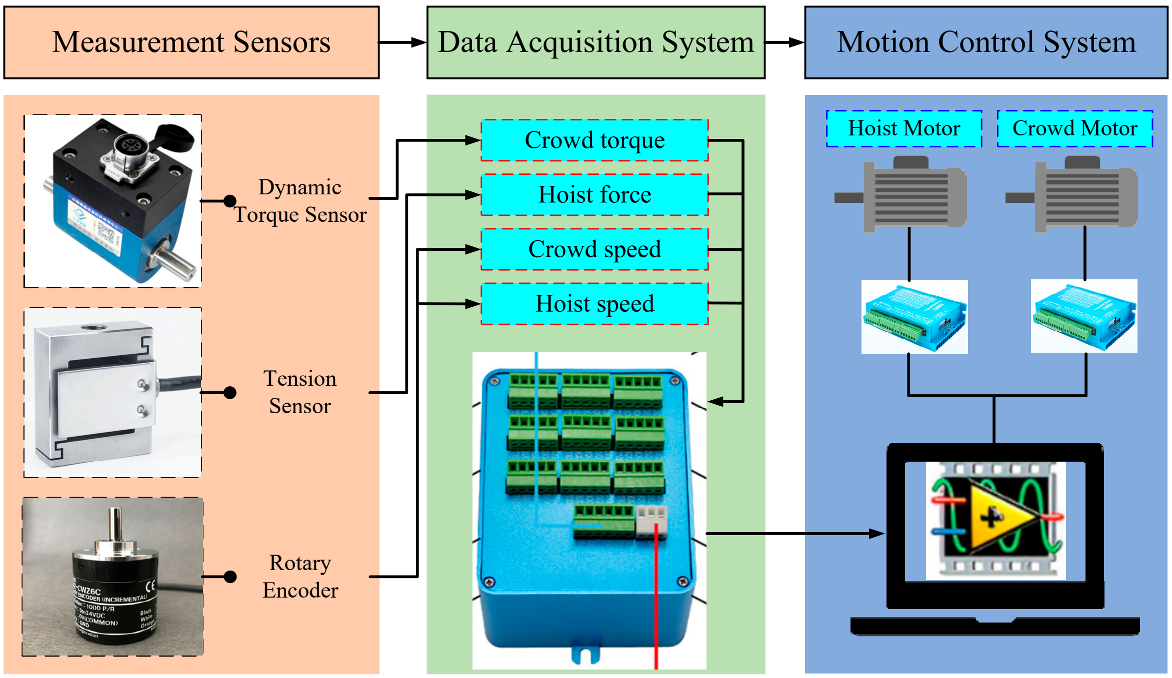

Figure 15. System structure of the electric shovel scale model test bench.

In order to ensure the reliability and stability of the measured data, the excavating test under various working conditions was repeated several times and the collected data were averaged. The data measured by the torque sensor and the tensile force sensor were processed via MATLAB to obtain the change curve of the excavating resistance with time.

Figures 16 and 17 show the simulation results and test results of the excavating resistance at different speed combinations and different repose angles, respectively. In order to display the change trend of excavating resistance more intuitively, polynomial fitting was performed on the data, and the original data were transparently processed. At the same time, in order to verify the feasibility of EDEM-RecurDyn bidirectional coupling simulation and the reliability of the results, the maximum excavating resistance and its occurrence time in the simulation and test are compared, and the correlation coefficient (R^2) is introduced to describe the matching degree between the simulation results and the test results, as shown in Table 7.

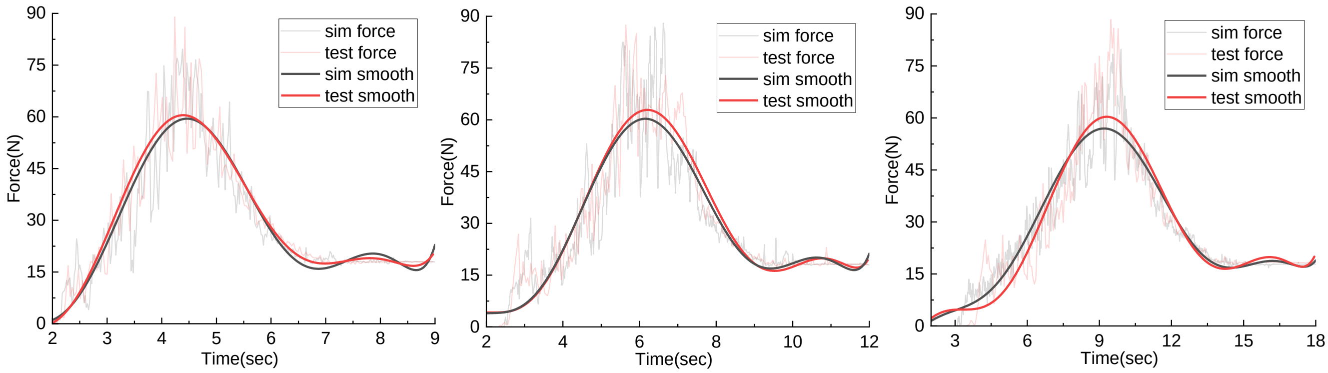

(**a**) (**b**) (**c**)

Figure 16. Comparison between simulation data and experimental data of excavation resistance under different speed combinations: (**a**) High-speed excavation; (**b**) Medium-speed mining; (**c**) Low-speed excavation.

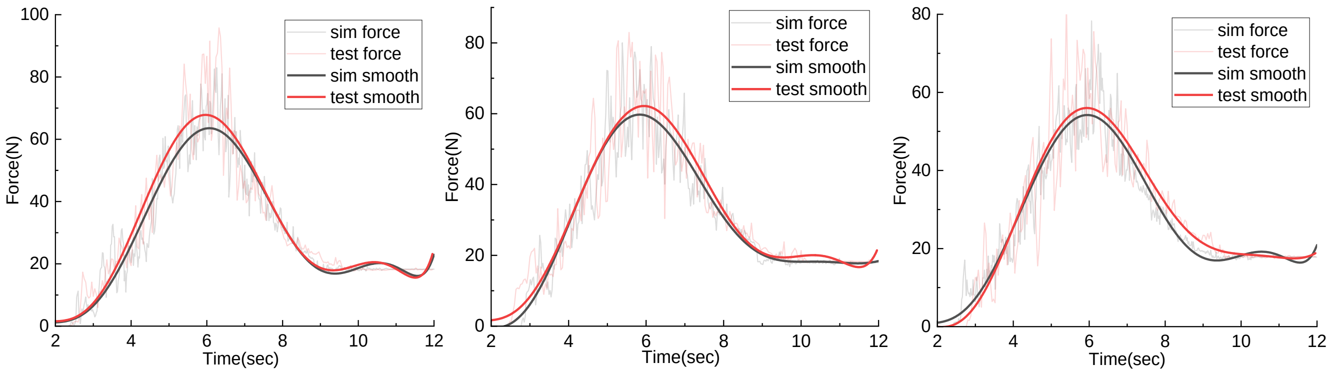

(**a**) (**b**) (**c**)

Figure 17. Comparison between simulation data and experimental data of excavation resistance under different pile angles: (**a**) 45° material surface excavation; (**b**) 40° material surface excavation; (**c**) 35° material surface excavation.

As can be seen from the table, under different working conditions, the simulation results of the maximum excavating resistance and the test results have a relative deviation of about 5%. The relative deviation of the maximum excavating resistance occurrence time is less than 2%. The R^2 value of the simulation results and the test results of excavating resistance is about 0.9, which shows a high degree of coincidence, indicating that the EDEM-RecurDyn bidirectional coupling simulation can accurately predict the excavation performance in the ECS excavating process.

Table 7. Comparison between simulation and experimental data under different working conditions.

Different Excavation Conditions	Maximum Excavating Resistance/N		Relative Deviation/%	Maximum Excavating Resistance Occurrence Time/s		Relative Deviation/%	Correlation Coefficient (R^2)
	Simulation Results	Test Results		Simulation Results	Test Results		
High-speed excavation	59.47	60.48	1.67	4.47	4.40	1.59	0.9473
Medium-speed excavation	60.31	62.88	4.09	6.15	6.23	1.28	0.9064
Low-speed excavation	56.95	60.33	5.60	9.19	9.34	1.61	0.8865
45° material surface excavation	63.54	67.82	6.31	6.07	5.96	1.85	0.8824
40° material surface excavation	59.74	62.17	3.91	5.84	5.94	1.68	0.9502
35° material surface excavation	54.20	55.99	3.20	5.95	5.91	0.68	0.8962

5. Conclusions

(1) In this paper, kinematic solution and force analysis of the excavating process of an ECS were carried out, a computer simulation method for excavating resistance based on EDEM-RecurDyn bidirectional coupling simulation was introduced, and the excavating process under different speed combinations and repose angles was simulated and analyzed.

(2) The excavation test was carried out by setting up and using an ECS scale model test bench, and the feasibility and reliability of the research method were verified by comparing the simulation results with the test results. The results show that the simulated excavating resistance was basically consistent with the excavating resistance measured by the test in terms of peak and change trend under various working conditions, which verifies that EDEM-RecurDyn bidirectional coupling simulation can accurately predict the excavating resistance of the ECS.

In addition, this research method can be fully used to optimize the excavating trajectory, excavating resistance, excavating efficiency and so on of the ECS in future work. On the other hand, the theoretical calculation of the excavating resistance can be verified by bidirectional coupling simulation, and the excavating resistance parameters in the theoretical method can also be modified by the simulation results, so as to obtain a more accurate theoretical calculation model of excavating resistance, and the research method is also applicable to various large mining machineries and excavating machinery.

Author Contributions: Conceptualization, Y.F. and C.G.; Data curation, Y.F. and B.L.; Funding acquisition, J.W.; Project administration, J.W.; Software, J.W.; Supervision, J.W.; Writing—Original draft, Y.F.; Writing—review and editing, Y.F. and J.W. All authors have read and agreed to the published version of the manuscript.

Funding: This research was funded by National Natural Science Foundation of China (Project No. U21A20125), Natural Science Foundation of Shanxi Province (Project No. 20210302124060).

Institutional Review Board Statement: Not applicable.

Informed Consent Statement: Not applicable.

Data Availability Statement: Not applicable.

Conflicts of Interest: The authors declare no conflict of interest.

References

1. Wei, B.; Gao, F.; Chen, J.; He, J.; Wu, S.; Song, Q. Mechanics performance of three-degree-of-freedom excavating mechanism of an electric shovel. *Proc. Inst. Mech. Eng. Part C J. Mech. Eng. Sci.* **2011**, *225*, 1443–1457. [CrossRef]
2. Zou, W.; Cheng, S.; Yang, L.; Zhou, H. Joint dynamic simulation of electric shovel working device EDEM-Adams-Simulink. *Comput. Aided Eng.* **2020**, *29*, 5.
3. Coetzee, C.J.; Basson, A.H.; Vermeer, P.A. Discrete and continuum modelling of excavator bucket filling. *J. Terramechanics* **2007**, *44*, 177–186. [CrossRef]

4. Coetzee, C.J.; Els, D. The numerical modelling of excavator bucket filling using DEM. *J. Terramechanics* **2009**, *46*, 217–227. [CrossRef]
5. Huang, P.P.; Xiao, X.Z. Simulation Study the Movement of Materials in Loader Shovel Working Process Based on EDEM. *Adv. Mater. Res.* **2013**, *655–657*, 320–325. [CrossRef]
6. Meng, Y.; Fang, H.; Liang, G.; Gu, Q.; Liu, L. Bucket Trajectory Optimization under the Automatic Scooping of LHD. *Energies* **2019**, *12*, 3919. [CrossRef]
7. Zhao, L.; Jin, X.; Liu, X. Numerical research on wear characteristics of drum based on discrete element method (DEM). *Eng. Fail. Anal.* **2019**, *109*, 104269. [CrossRef]
8. Zhao, L.; Wang, Y.; Zhang, M.; Jin, X.; Liu, H. Research on self-adaptive cutting control strategy of shearer in complex coal seam. *J. China Coal Soc.* **2022**, *47*, 541–563.
9. Bi, Q.; Wang, G.; Wang, Y.; Yao, Z.; Hall, R. Digging Trajectory Optimization for Cable Shovel Robotic Excavation based on a Multi-Objective Genetic Algorithm. *Energies* **2020**, *13*, 3118. [CrossRef]
10. Wu, J.; Wang, G.; Bi, Q.; Hall, R. Digging force and power consumption during robotic excavation of cable shovel: Experimental study and DEM simulation. *Int. J. Min. Reclam. Environ.* **2020**, *35*, 12–33. [CrossRef]
11. Zhang, T.; Fu, T.; Song, X.; Qu, F. Multi-objective excavation trajectory optimization for unmanned electric shovels based on pseudospectral method. *Autom. Constr.* **2022**, *136*, 104176. [CrossRef]
12. Wang, X.; Sun, W.; Li, E.; Song, X. Energy-minimum optimization of the intelligent excavating process for large cable shovel through trajectory planning. *Struct. Multidiscip. Optim.* **2018**, *58*, 2219–2237. [CrossRef]
13. Wang, H.; Lu, X.; Sheng, C.; Zhang, Z.; Cui, W.; Li, Y. General frame for arbitrary 3R subproblems based on the POE model. *Robot. Auton. Syst.* **2018**, *105*, 138–145. [CrossRef]
14. Mckyes, E. *Soil Cutting and Tillage*; Elsevier: Amsterdam, The Netherlands, 1985; Volume 7.
15. Rasimarzabadi, R.; Joseph, T. Particle flow mechanism into cable shovel dippers. *J. Terramechanics* **2016**, *64*, 10–22. [CrossRef]
16. Kostic, S.; Trivan, J. Optimization of coal overburden excavation considering variable geomechanical properties and states of excavator teeth. *Arch. Min. Sciences.* **2022**, *1*, 123–142.
17. Kostic, S.; Vasovic, N.; Jevremovic, D. Stability of earth slopes under the effect of main environmental properties of weathered clay-marl deposits in belgrade (serbia). *Environ. Earth Sci.* **2016**, *75*, 492. [CrossRef]
18. Xia, Y.; Yang, M.; Lin, L.; Ji, Z.; Zhu, Z. Effect of Blade Angles on the Shovel Muck Capacity and Wear Characteristics for TBM Scraper. *Arab. J. Sci. Eng.* **2021**, *46*, 5203–5218. [CrossRef]
19. Huang, W.; Zhao, D.; Liu, C.; Meng, X.; Wenhao, D.U. Optimization of Garlic Digging Shovel Parameters Based on EDEM and Quadratic Regression Orthogonal Rotation Combination Design. In Proceedings of the 2020 3rd World Conference on Mechanical Engineering and Intelligent Manufacturing (WCMEIM), Shanghai, China, 4–6 December 2020.
20. Wang, S.; Yu, S.; Hou, L.; Wu, B.; Wu, Y. Prediction of Bucket Fill Factor of Loader Based on Three-Dimensional Information of Material Surface. *Electronics* **2022**, *11*, 2841. [CrossRef]
21. Wang, S.; Yin, Y.; Wu, Y.; Hou, L. Modeling and Verification of an Acquisition Strategy for Wheel Loader's Working Trajectories and Resistance. *Sensors* **2022**, *22*, 5993. [CrossRef]
22. Bi, Q.; Wang, G.; Chen, L.; Huang, T.; Li, A.; Li, G.; Li, X. Simulation and test of mechanical excavator digging resistance based on discrete element-multibody dynamics co-simulation. *J. Jilin Univ. Eng. Ed.* **2019**, *1*, 106–116. [CrossRef]
23. Bi, Q.; Wang, G.; Yang, R.; Liu, Y.; Lu, Y.; Xing, S. Study on theory and methods of payload online estimation for cable shovels. *J. Braz. Soc. Mech. Sci. Eng.* **2019**, *41*, 53. [CrossRef]
24. Quist, J.C. DEM Modelling and Simulation of Cone Crushers and High Pressure Grinding Rolls. Ph.D. Thesis, Chalmers University of Technology, Gothenburg, Sweden, 2017.
25. Fan, Z.; Zhang, T.; Qiao, J.; Li, G.; Zhao, Y.; Wang, X.; Sun, W.; Song, X. Multi-objective Excavation Trajectory Optimization for Intelligent Electric Shovel Based on ROS. *IOP Conf. Ser. Mater. Sci. Eng.* **2020**, *717*, 112–120. [CrossRef]
26. Wang, D.; Zhang, J.; Guo, H.; Liu, R.; Kou, Z. Design of a 2T1R-Type Parallel Mechanism: Performance Analysis and Size Optimization. *Actuators* **2022**, *11*, 262. [CrossRef]